



HAL
open science

Dissolved organic matter biodegradation along a hydrological continuum in permafrost peatlands

Daheydrey Payandi-Rolland, Liudmila Shirokova, Marwa Tesfa, Pascale Benezeth, Artyom Lim, Daria Kuzmina, Jan Karlsson, Reiner Giesler, Oleg S Pokrovsky

► To cite this version:

Daheydrey Payandi-Rolland, Liudmila Shirokova, Marwa Tesfa, Pascale Benezeth, Artyom Lim, et al.. Dissolved organic matter biodegradation along a hydrological continuum in permafrost peatlands. Science of the Total Environment, 2020, 749, pp.141463. 10.1016/j.scitotenv.2020.141463. hal-03004367

HAL Id: hal-03004367

<https://hal.science/hal-03004367>

Submitted on 16 Nov 2020

HAL is a multi-disciplinary open access archive for the deposit and dissemination of scientific research documents, whether they are published or not. The documents may come from teaching and research institutions in France or abroad, or from public or private research centers.

L'archive ouverte pluridisciplinaire **HAL**, est destinée au dépôt et à la diffusion de documents scientifiques de niveau recherche, publiés ou non, émanant des établissements d'enseignement et de recherche français ou étrangers, des laboratoires publics ou privés.

- 26 • BDOC ranged from 0 to 20% and could at the most account for 10% of CO₂ emissions
- 27 from surface waters of these permafrost peatlands

28

29

30 **Abstract**

31 Arctic regions contain large amounts of organic carbon (OC) trapped in soil and wetland
32 permafrost. With climate warming, part of this OC is released to aquatic systems and degraded
33 by microorganisms, thus resulting in positive feedback due to carbon (C) emission. In wetland
34 areas, water bodies are spatially heterogenic and separated by landscape position and water
35 residence time. This represents a hydrological continuum, from depressions, smaller water
36 bodies and lakes to the receiving streams and rivers. Yet, the effect of this heterogeneity on the
37 OC release from the soil and its processing in waters is largely unknown and not accounted for
38 in C cycle models of Arctic regions. Here we investigated the dissolved OC (DOC)
39 biodegradation of aquatic systems along a hydrological continuum located in two discontinuous
40 permafrost sites: in western Siberia and northern Sweden. The biodegradable dissolved OC
41 (BDOC₁₅; % DOC lost relative to the initial DOC concentration after 15 days incubation at
42 20°C) ranged from 0 to 20% for small water bodies located at the beginning of the continuum
43 (soil solutions, small ponds, fen and lakes) and from 10 to 20% for streams and rivers. While
44 the BDOC₁₅ increased, the removal rate of DOC decreased along the hydrological continuum.
45 The potential maximum CO₂ production from DOC biodegradation was estimated to account
46 for only a small part of *in-situ* CO₂ emissions measured in peatland aquatic systems of northern
47 Sweden and western Siberia. This suggests that other sources, such as sediment respiration and
48 soil input, largely contribute to CO₂ emissions from small surface waters of permafrost
49 peatlands. Our results highlight the need to account for large heterogeneity of dissolved OC
50 concentration and biodegradability in order to quantify C cycling in arctic water bodies
51 susceptible to permafrost thaw.

52

53 **1. Introduction**

54 The carbon (C) released from thawing permafrost is biotically and abiotically processed in
55 aquatic systems (Abbott et al., 2016; Cory and Kling, 2018; Mann et al., 2015). However, the
56 degree and intensity of this processing are strongly variable both in space (local to global scale)
57 and time (day/night to season) and not explicitly accounted for in global modelling of
58 permafrost-carbon-climate feedback. The spatial variability includes the various types of water
59 bodies of those regions, all belonging to the hydrological continuum (Figure 1). Globally, the
60 concept of ‘hydrological continuum’ (Creed et al., 2015; Palmer et al., 2016) includes the
61 movement of water from sources (soil and supra-permafrost waters) to intermediate reservoirs
62 (lakes and streams) and finally into terminal reservoirs (large rivers and their estuaries). In
63 Arctic regions, the hydrological continuum (HC) is highly dependent on the maturation cycle
64 of water bodies. All steps of HC are especially important as they can influence the biochemical
65 properties, photo- (Panneer Selvam et al., 2019) and bio-degradability (Liu et al., 2019; Vonk
66 et al., 2015) of dissolved organic matter (DOM). Since the transport of thawed permafrost
67 organic C can spatially relocate the emissions of greenhouses gases (Vonk and Gustafsson,
68 2013), the heterogeneity of waterbodies observed along a hydrological continuum is a key point
69 to understand the C cycle in these regions.

70 Dissolved organic carbon (DOC) is the main form of terrestrial organic carbon (OC) exported
71 to soil solution, rivers, wetlands and lakes (Chapin et al., 2006; Cole et al., 2007). This is
72 especially true in the case of discontinuous permafrost regions, where the hydrologic flow paths
73 have longer residence times and allow a greater degree of DOC processing during lateral
74 transport (Olefeldt and Roulet, 2014, 2012; Tang et al., 2018; Walvoord and Striegl, 2007). For
75 these reasons, coupled aquatic-soil studies of organic matter (OM) in continuous-discontinuous
76 permafrost regions are needed (Vonk et al., 2019). The importance of surface waters from
77 frozen peatlands in DOC processing and CO₂ emissions motivated numerous studies of aquatic

78 DOM (Hulatt et al., 2014; Manasypov et al., 2015; Mann et al., 2015, 2012; Peura et al., 2020;
79 Pokrovsky et al., 2016; Shirokova et al., 2019). The latter study in NE European tundra
80 peatlands demonstrated weak biodegradation of DOM along a hydrological continuum from
81 peatland subsidence to a large river (Pechora) and suggested that CO₂ emission from surface
82 waters could be explained either by sediment respiration or by fast processing of fresh supra-
83 permafrost flow delivered from peat pore water and thawing soil ice. As such, to quantify
84 overall DOM biodegradation potential in Arctic peatland waters, it is necessary to study the full
85 continuum of surface fluids, from the soil and supra-permafrost waters to large lakes or river
86 systems using universal techniques over large geographic coverage (Ma et al., 2019).

87 This study aimed to quantify the magnitude and controlling factors of DOM biodegradation
88 potential along a hydrological continuum from soil water to medium-sized rivers and lakes
89 located in a discontinuous permafrost area in western Siberia and northern Sweden. Strong
90 seasonal variability in the high latitude C cycle is well known (Gao et al., 2019; Li et al., 2019).
91 Yet, this study was carried out during baseflow period (July to October) when the quality and
92 quantity of the DOC in waters are most stable (Chupakov et al., 2020; Holmes et al., 2012;
93 Manasypov et al., 2015; Neff et al., 2006; Olefeldt and Roulet, 2012; Tang et al., 2018). Our
94 working hypothesis is that the BDOC decreases along the HC (with the preferential degradation
95 of easily biodegradable C molecules) and that the amplitude of this decrease depends on
96 landscape context and the DOM origin. To test this hypothesis, we carried out aerobic
97 biodegradation experiments (following Vonk et al. (2015)) and monitored resulting changes in
98 DOM quantity and quality. We further compared the possible contribution of DOM
99 biodegradation along the HC to published CO₂ emission from the surface waters representative
100 of the study regions.

101

102 **2. Materials and methods**

103 *2.1. Geographical, climatic and hydrological setting of sampling sites*

104 In high latitude continental planes, the permafrost thaw leads to the formation of
105 “thermokarst” (thaw) lakes resulting from the soil ice melt and the permafrost subsidence in
106 frozen wetlands. The formation and development of thermokarst lakes appeared to follow a
107 cycle (Kirpotin et al., 2009; Pokrovsky et al., 2011) and is an important part of the hydrological
108 continuum of the region (Figure 1). The cycle starts with the subsidence of thawing soil forming
109 a depression and filled by high molecular weight OM rich thaw water. The size of the depression
110 grows due to the ongoing subsidence of peat soil and the active abrasion of edges until it reaches
111 a lake size (thermokarst lake) with stable edges, that can be eventually drained into another lake
112 or streams and rivers. The vegetation can then colonize the drained lake bottom and gradually
113 the permafrost will be renewed, and the cycle can start over again by the formation of a wet
114 depression. Lichens mostly dominate in mounds, while sphagnum type colonizes depressions,
115 and graminoids can be found in fens and drained lakes.

116 The two selected study sites are located in the arctic/subarctic region, within a discontinuous
117 permafrost area. Their detailed description can be found elsewhere (Åkerman and Johansson,
118 2008; Brown et al., 1997; Raudina et al., 2018). The Siberian study site (referred to as
119 Khanymey, Figure S1 A in supplementary), is located near the town of Khanymey (63°47' N;
120 75°32' E) in a northern taiga, with a mean annual temperature of -5.6 °C and precipitation of
121 540 mm. The palsas peat bogs have a peat thickness of 0.1 to 1.4 m and the active (unfrozen)
122 layer thickness (ALT) is around 90 and 215 cm under the surface of mounds and hollows,
123 respectively. The vegetation on the mounds is dominated by dwarf shrubs (*Ledum* ssp., *Betula*
124 *nana*, *Andromeda polifolia*, *Vaccinium* ssp., *Empetrum nigrum*), lichens (*Cladonia* ssp.,
125 *Cetraria*, *Ochrolechia*) and mosses, while the hollows are covered by moss-sedge associates
126 (grasses *Eriophorum russeolum*, *E. vaginatum*, *Carex rotundata*, *C. limosa*, *Menyanthes*

127 *trifoliata*, *Comarum palustre*; mosses *Sphagnum. balticum*, *S. majus*, *S. lindbergii*, *S.*
128 *warnstorffii*) and dwarf shrubs, such as *Oxycoccus palustris* (Raudina et al., 2018). In
129 Khanymey, we have chosen seven locations that belonged to a HC. They were sampled in July
130 2018 and used as substrates for incubation. We sampled two supra-permafrost waters from
131 peatland, one on a mound and one on a hollow (see sampling details in Raudina et al., 2018);
132 two lakes: organic-rich Chernoe and organic-poor Trisino; two streams: the one close to the
133 outlet of the lake and another one located far from this outlet (Lybydyakha); and finally one
134 medium-size river Pyakopur that flows through peatland and forest (Ala-aho et al., 2018).
135 Localization, surface, depth and physicochemical parameters of the seven sampled locations
136 are presented in the supplementary Table S1.

137 The second site is the Stordalen mire (68°21' N and 19°02' E) located in the vicinity of
138 Abisko in Northern Sweden (Figure S1 B). The ALT in the mire is approximately 0.5 to 1 m
139 thick (Åkerman and Johansson, 2008; Klaminder et al., 2008) and composed of 0.5 m of peat
140 (Malmer et al., 2005) that overlays silty lacustrine sediment that has a glacial origin at depth
141 (Klaminder et al., 2008). The mean annual temperature is -0.7 °C (Kohler et al., 2006) and the
142 annual precipitation is 299 mm (Petrescu et al., 2007). The Stordalen mire is an ombrotrophic
143 palsa that rises above semi-wet and wet minerotrophic fens, streams and shallow lakes (Wik et
144 al., 2013). The hummock (*i.e.* the equivalent of mound structure in the Khanymey site)
145 vegetation is dominated by lichens (*Cladonia* spp. and *Cetraria* spp. and mosses, such as
146 *Sphagnum balticum* (Russ.) C. Jens.) in the bottom layer while *Eriophorum vaginatum* and
147 *Empetrum hermaphroditum* dominated in the field layer. In the hollows, the field layer is
148 dominated by graminoids such as *Carex rotundata*, *E. vaginatum* and *E. angustifolium* while
149 the bottom layer consists of mosses, such as *S. balticum*, *S. fuscum* and carpet Bryatae (Malmer
150 et al., 2005). Seven locations were sampled in the Stordalen mire in October 2018, before
151 snowfall and ice-on: the soil solution of a hummock, the water from a crack at the edge of a

152 small pond, the small pond itself, a fen, a lake (Villasjön, [Wik et al. \(2013\)](#)) and two streams,
153 a proximal one, near the outlet of the lake and a distal one located at the border of the mire.
154 Localization, surface, depth and physicochemical parameters of the seven sampled locations
155 are presented in Table S1. In the case of soil solution samples, a pit was made on hummock
156 (/mound) or hollow. After a few minutes, gravitational (supra-permafrost) water from the
157 surrounding soils was accumulated in the pit. This supra-permafrost water has been used for
158 the experiment and named “soil solution” in the rest of this study.

159

160 *2.2. Experimental setup*

161 Each water sample was collected directly in a MilliQ-rinsed Nalgene® bottle and
162 processed in less than 12 h after sampling following the protocol of [Vonk et al. \(2015\)](#) and
163 [Shirokova et al. \(2019\)](#), employing the same filter units and membranes. All the manipulations
164 were performed under sterile conditions. Waters collected in the field were first filtered through
165 pre-combusted (4 hours at 450°C) GF/F filters (Whatman, nominal pore diameters: 0.7 µm,
166 diameter 47 mm) using sterile filtration units (Millipore, 250 mL) and then incubated in sterile
167 60 mL amber glass bottles at 20 ± 2 °C, without light exposure. To keep oxygenic conditions
168 in incubation bottles, bottle caps were not completely tightened and bottles were manually
169 shaken at least every two days. Each sampling included filtration through pre-combusted GF/F
170 filters mounted on a Sartorius filter unit (25 mm diameter). The duration of incubation depended
171 on field logistics and ranged from 30 days in Siberian waters to 15 days in Northern Sweden.
172 Information on sampling date, replicate and the type of conducted analyses are listed in Table
173 S2.

174

175 *2.3. Analyses*

176 The pH (uncertainty of ± 0.01 pH units), conductivity (± 0.1 µS cm⁻¹) and absorbance
177 (250 to 500 nm, 1 nm step; SpectraMax M5e Molecular Devices in Stordalen, and Eppendorf

178 BioSpectrometer® basic in Khanymey) were measured within 1 h after the sampling. Fixation
179 and/or storage methods for each type of delayed analysis are listed in Table S2. Water samples
180 for DOC and fluorescence analyses were adjusted around pH = 2 using HCl, which removed
181 the dissolved inorganic carbon (DIC) and minimize the quenching of fluorescence caused by
182 metal complexation (McKnight et al., 2001). Fluorescence was measured according to Roehm
183 et al. (2009) on a SpectraMax M5e. DOC and DIC were measured by a high-temperature
184 thermic oxidation method using a Shimadzu TOC-VSCN analyzer, with an uncertainty of 2%.
185 Organic acids and anions were measured by high-performance ionic chromatography (Dionex
186 Ics-5000⁺). Total bacterial cells (TBC) concentration was measured by flow cytometry
187 (Guava® EasyCyte™ systems, Merck) using 1 µL of 10 times diluted SYBR GREEN (Merck)
188 marker, added to 250 µL of each sample before analysis. The typical uncertainty on these
189 measurements was between 10 and 20%.

190

191 2.4. Data treatment

192 The biodegradability of DOC (BDOC) was determined using commonly used equations
193 proposed by Vonk et al. (2015) (Table S3). This gives the relative proportion of the
194 biodegradable DOC in relation to the initial DOC concentration (Table S3). The apparent
195 removal rate of DOC (RDOC) was calculated as the slope of linear regression for the incubation
196 time (RDOC, Table S3). As the biodegradation of Khanymey and Stordalen did not last the
197 same amount of time (respectively 30 and 15 days), in the rest of the article the RDOC and
198 BDOC values were calculated at 15 days of incubations to allow a direct comparison between
199 the two sites (*i.e.* BDOC₁₅ and RDOC₁₅). Absorbance data (Peacock et al., 2014; Weishaar et
200 al., 2003) were used to assess the (i) the molecular weight of the DOC by the weight average
201 molecular weight index (WAMW), (ii) the humification of DOM by the E2:E4 ratio and (iii)
202 the relative amount of aromatic components by the specific UV absorbance at 254 nm

203 (SUVA₂₅₄) (Table S3). The Fluorescence index (FI) (McKnight et al., 2001), was calculated to
204 separate DOC from a terrestrial origin (FI<1.4) than DOC from a microbial origin (FI > 1.4,
205 Cory et al., 2010; Roehm et al., 2009) as detailed in Table S3.

206 Statistical treatment of the data included least-square linear regression and Pearson
207 correlation to assess the evolution of parameters during incubation. To compare the
208 biodegradation in waters within and between each HC principal component analysis (PCA) was
209 used. Input data included initial chemical and biological parameters of waters that are
210 hypothesized to contribute to the variation of BDOC₁₅ and RDOC₁₅ of waters: DOC, TBC,
211 WAMW, E2:E4 ratio, pH, PO₄-P, SUVA₂₅₄, conductivity and some organic acids
212 concentrations (acetate, lactate and formate). The statistics were performed using R software
213 (version 3.6.1) with “FactoMineR” and “factoextra” packages. All measured incubation
214 parameters are provided in the Mendeley Data Repository (Payandi-Rolland, 2020).

215

216 **3. Results**

217 *3.1 Inorganic water chemistry at the beginning of incubation*

218 In Khanymey water at day 0 of incubation, the pH increased along the HC (from soil
219 solution - mound at 4.2 to the Pyakopur river at 6.0). Specific conductivity ranged from 15 to
220 47 $\mu\text{S cm}^{-1}$ in the proximal stream and in the soil solution sampled at the mound, respectively.
221 The DIC concentration of all waters was lower than 1.1 mg L^{-1} (supplementary Table S1). In
222 Stordalen, the pH of waters increased along the HC (from 4.1 at the crack to 7.2 at the distal
223 stream and Villasjön Lake). The specific conductivity ranged from 26 to 100 $\mu\text{S cm}^{-1}$ in the fen
224 and in the soil solution from the hummock, respectively. The DIC concentrations ranged from
225 1.7 (small pond) to 4.6 mg L^{-1} (proximal stream; supplementary Table S1).

226

227 3.2 Biodegradation of DOC

228 The DOC concentration of the Khanymey site showed high initial DOC values for
229 waters located at the beginning of the HC (*i.e.* soil solution at the mound and hollow, and the
230 Lake Chernoe, Figure 2 A.1). The DOC concentrations at the end of HC (*i.e.* lake Trisino,
231 proximal and distal stream, and the Pyakopur River) were much lower and ranged between 14.5
232 and 16.7 mg L⁻¹. The DOC concentrations showed a significant linear decrease ($p < 0.05$, R²
233 ranging between 0.45 to 0.69) in all incubations, except for the soil solution from the hollow
234 and both thermokarst lakes (Figure 2 A.1). The corresponding BDOC value increased in all
235 incubations from day 0 to 30 (Figure 2 B.1). After 15 days of the experiment, the lowest
236 BDOC₁₅ value was $-0.4 \pm 2.3\%$ for the soil solution from the mound and the highest was 21.9
237 $\pm 4.9\%$ for the Trisino Lake (Figure 3). The rates of DOC removal over 15 days (RDOC₁₅) with
238 the highest rates in the soil solution from the hollow (0.61 ± 0.1 mg L⁻¹ d⁻¹), and the lowest in
239 lake Chernoe (-0.11 ± 0.1 mg L⁻¹ d⁻¹) (Figure 3 and Table S5). Soil solution from the mound
240 exhibited the highest concentration of low molecular weight organic acids (LMWOA), *i.e.*
241 formate, lactate and acetate (Table S4). Initial values of bacterial cell numbers (TBC) ranged
242 from 2.89×10^5 (Trisino Lake) to 1.43×10^6 cells mL⁻¹ (distal stream) (Table S1). During the
243 incubation, the bacterial concentration increased by 30% of the initial amount in the soil
244 solution from the mound to 72% in the incubation of the distal stream (data not shown).

245 The DOC concentrations in the Stordalen waters were high at the beginning of the
246 continuum (soil solution, hummock and crack), then decreased in the small pond, and became
247 lower at the end of the continuum (fen, Villasjön Lake, proximal and distal stream) (Figure 2
248 A.2). The DOC concentrations significantly decreased during incubations. The corresponding
249 BDOC values increased in all incubations from day 0 to 15 (Figure 2 B.2). The BDOC₁₅ ranged
250 between 10.5 - 19.9% with the lowest values in the proximal stream and the crack, and the
251 highest in the distal stream (Figure 3). The waters located at the beginning of the continuum

252 exhibited the highest RDOC₁₅ while the lower RDOC₁₅ values were observed for end-members
253 of the HC (Figure 3 and Table S5). As for the Khanymey continuum, soil solution from the
254 hummock contained much higher initial concentrations of acetate and formate compared with
255 other incubated waters (Table S4). During incubation, only the soil solution from the hummock
256 showed a decrease (78%) in acetate concentrations. The initial TBC ranged from 2.26×10^3
257 (distal stream) to 3.76×10^4 cells mL⁻¹ (crack) (Table S1). During the incubation period, the
258 lowest increase in TBC was obtained for the Villasjön Lake (49%) and the highest increase was
259 measured for the distal stream (by a factor of 25, data not shown).

260

261 *3.3 DOM optical properties*

262 In the Khanymey continuum, the SUVA₂₅₄ ranged between 3.4 L mg C⁻¹ m⁻¹ for the
263 proximal stream to 4.2 L mg C⁻¹ m⁻¹ for the river (Figure 2 C.1). The SUVA₂₅₄ increased in all
264 samples during the incubations, with the lowest increase for the soil solution – mound (14%)
265 and highest for the proximal stream (60%). The ratio E2:E4 increased with incubation time at
266 the beginning of the continuum (both soil solutions and the Chernoe Lake) and decreased with
267 time in waters located at the end of HC (from the Trisino lake to the Pyakopur River) (Figure
268 S2 A.1). Normalized molecular weight (WAMW) allowed distinguishing 2 groups of samples
269 (Figure S2 B.1). The first one included soil solutions from the mound and hollow and the
270 Chernoe Lake, with stable values ranging between 516 - 526 and 526 - 540 Da from the
271 beginning to the end of the incubation, respectively. The second group comprised all other water
272 types of the continuum, with WAMW values increasing from 558 - 586 Da to 590 - 679 Da
273 during the incubations.

274 In the Stordalen hydrological continuum, the SUVA₂₅₄ ranged between 2.9 and 4.9 L
275 mg C⁻¹ m⁻¹ at the beginning to 3.3 and 5.1 L mg C⁻¹ m⁻¹ at the end of the experiment (Figure 2
276 C.2). An increase in SUVA₂₅₄ of 12, 19 and 22% was observed during the incubation of the soil

277 solution – hummock, proximal and distal stream. For the remaining samples of the Stordalen
278 continuum, the increase in SUVA₂₅₄ was below 10%. The evolution of the ratio E2:E4 during
279 incubations separated the systems in two groups (Figure S2 A.2), i.e. one with stable values at
280 the beginning of the HC (*i.e.* crack, small pond, fen, and soil solution), and one with oscillating
281 values at the end of the HC (*i.e.* both streams and the lake). The lowest WAMW values were
282 recorded for soil solution - hummock and crack with the initial and final values of 506-511 and
283 513-515 Da, respectively (Figure S2 B.2). The highest values of WAMW were obtained for the
284 small pond and the proximal stream (initial: 625 to 716 Da, final: 662 to 779 Da). The
285 fluorescence index (FI) of waters in the Stordalen HC ranged between 1.52 and 2.23 at the
286 beginning of incubation for the crack and the distal stream, respectively (Figure 2 D). FI values
287 decreased for all waters during incubation, with values < 1.40 for the crack, the small pond and
288 the fen and slightly higher values for the proximal stream (1.67 ± 0.2) after 5 days of incubation.

289

290 *3.4 PCA results*

291 The principal component analysis (PCA) performed on data from both hydrological
292 continuums (Figure 4 and Table S6) showed that the component number 1 (PC1) explained
293 34.0% of the variation, with an important contribution of conductivity, DOC concentration,
294 RDOC₁₅ and organic acids concentrations (acetate and formate). The PC2 explained 26.9% of
295 the variations, with the largest contribution coming from E2:E4 ratio, SUVA₂₅₄, pH and
296 LMWOA concentration. The BDOC₁₅ appeared to be grouped with the pH and the E2:E4 ratio,
297 whereas lactate, DOC, and SUVA₂₅₄ were on the opposite side of the plot. Acetate and formate
298 concentrations and specific conductivity were grouped tight. No clear visual separation by study
299 site could be seen. However, the end-member waters of both continuums were clustered in the
300 upper left quadrant of the plot, while other waters, except the soil solution from the mound of
301 Khanymey, were mostly located in the lower right quadrant.

302

303 **4. Discussion**

304 *4.1 Evolution of the DOC removal rate and biodegradability along the hydrological* 305 *continuum*

306 The decreasing trend of RDOC₁₅ values observed along the HC, and the inverse trend
307 for BDOC₁₅ values (Figure 3) suggest that the soil waters located at the beginning of the
308 continuum contain rapidly processed DOC, while the lake and river waters, at the end of HC,
309 contain slowly processed DOC. Drastic differences in RDOC₁₅ between the beginning and the
310 end of the HC suggest that these changes across pore waters, supra-permafrost waters, surface
311 small ponds and depressions of frozen peatlands, are primarily controlled by water residence
312 time (Catalán et al., 2016; Obernosterer and Benner, 2004). Indeed, when the residence time of
313 water is short, the decay rate of OC is believed to be governed by photo-degradation and
314 flocculation of OC (Catalán et al., 2016; Evans et al., 2017). Moreover, the labile parts of the
315 DOM are likely to be firstly processed during the transition because the fresher DOC is
316 delivered into the early stages of the HC.

317 The BDOC₁₅ of streams and rivers in both continuums ranged between 10 to 20%
318 (Figure 3) which is generally consistent with the values obtained for Arctic riverine systems
319 (typically 10 to 40%, Holmes et al., 2008; Mann et al., 2012; Wickland et al., 2012) and for
320 waters of thawing and collapsing permafrost (10 to 40%, Abbott et al., 2014). Soil solutions,
321 crack, small pond, fen and lake waters had a BDOC₁₅ ranging between 0 and 20%, which is
322 consistent with the biodegradability of lake waters from the Stordalen mire (10 to 20%, Roehm
323 et al., 2009). However, the biodegradability of fen leachate in the latter study ranged between
324 50 and 60%, which is 4 times higher than our values for the fen (~15%). Presumably, the fresh
325 leachate used by Roehm et al. (2009) contained a higher concentration of bioavailable OM
326 compared with natural, partially processed, fen waters used in this and other studies (*i.e.*
327 Michaelson et al., 1998; Spencer et al., 2015; Wickland et al., 2007). The BDOC₁₅ values across

328 the two continuums of this study are at the highest range of those reported in the HC of frozen
329 peatlands of Northern Eurasia (between 0 to 10% for depression, thermokarst lake, river and
330 stream, [Shirokova et al., 2019](#)) and also slightly higher than the BDOC of waters from
331 discontinuous permafrost (5 to 15%, mean 14%) ([Vonk et al., 2015](#)).

332 The PCA analysis allowed distinguishing two trends of biodegradability behavior linked
333 to LMWOA: *i*) the BDOC₁₅, which negatively correlated with lactate but was not linked to
334 acetate and formate, and *ii*) the RDOC₁₅; positively correlated to acetate and formate but which
335 did not correlate with lactate. This could suggest that the initial concentration of acetate and
336 formate influences the removal rate of DOC, because their presence triggers intensive microbial
337 metabolism as it was also observed by [Cappenberg et al. \(1982\)](#). In contrast, the overall
338 biodegradability of waters may be linked to the pattern of lactate which dominated in
339 concentrations of LMWOA of both continuums.

340

341 *4.2 Evolution of the DOC quality along the hydrological continuum*

342 The positive and negative correlation between E2:E4 spectral ratio and SUVA₂₅₄
343 respectively, with BDOC₁₅ observed by the PCA analysis (Figure 4), implies that an increase
344 in the humification of DOM and a decrease in the concentration of aromatic components
345 increase the biodegradable potential of DOM. The grouping of individuals waters located at the
346 end of both continuums in the upper left quadrant of the PCA biplot suggests that they are
347 influenced by the same variables (WAMW, TBC, pH and E2:E4 ratio). This is not observed for
348 waters at the beginning of continuums, whose signals were widely spread on the biplot. Such a
349 grouping of waters can be due to the mixing of large water bodies, receiving mostly lateral
350 surface flow due to precipitation, while smaller water bodies are mainly supplied by lateral
351 surface and supra-permafrost flow from thawing permafrost (Figure 1).

352 For the Stordalen continuum, a decreasing trend of FI in the course of incubation of
353 each water of the HC (Figure 2 D) indicates either *i*) an increase in the terrestrially-derived OM
354 or *ii*) a decrease in the microbially-derived OM (Cory et al., 2010; Mann et al., 2012). As no
355 fresh vegetation leachate was added in our incubations, the observed decrease of FI values
356 during the incubation of Stordalen waters corresponds to a relative decrease in the amount of
357 microbially-derived OM compared to the overall amount of OM. This is at odds with the
358 reported resistance of the bacterially-derived OM to the microbial degradation in freshwater
359 (Kawasaki et al., 2013). We, therefore, hypothesize that the relative decrease of the microbially-
360 derived OM occurred due to a lack of easily biodegradable terrestrial OM and the persistence
361 of the most recalcitrant part of terrestrial OM, which is consistent with an increase in SUVA₂₅₄
362 and WAMW with the incubation time. Moreover, a recent study on the evolution of the DOM
363 along a soil-stream-river continuum (Hutchins et al., 2017) demonstrated that soil-stream
364 waters were a hot spot of DOM degradation, with selective removal of low molecular weight
365 (LMW) components, whereas stream-river waters were more dominated by the degradation of
366 humic-like aromatic components. This trend is also observed in our study, particularly for the
367 Khanymey continuum in which the E2:E4 ratio (a proxy for humification degree) increased
368 during incubation of waters located at the beginning of the HC and decreased with time for the
369 waters at the end of the HC (Figure S2 A.1). This is also in agreement with the rapid uptake of
370 LMWOA observed during incubation (Table S4). SUVA₂₅₄ of the Khanymey and Stordalen
371 HC (up to 6.3 and 5.5 L mg C⁻¹ m⁻¹, respectively) are greater than most of the previously
372 reported data of waters from depressions, lakes and river of discontinuous permafrost area (3.3
373 to 4.4 L mg C⁻¹ m⁻¹ (Roehm et al., 2009; Shirokova et al., 2019), but comparable to the values
374 of permafrost leachate (6.6 ± 0.1 L mg C⁻¹ m⁻¹, Roehm et al.; 2009). Such high SUVA values
375 reflect the dominance of allochthonous DOM of peat, providing the majority of DOC input to
376 the water bodies.

377

378 *4.3 Comparison between the hydrological continuum of Khanymey and Stordalen*

379 We note that there are somewhat higher levels of BDOC₁₅ in waters from the Stordalen
380 peat mire compared with the Khanymey peatlands (10 to 20% and 0 to 20%, respectively,
381 Figure 3). This difference cannot be attributed to the difference in seasons of sampling (July in
382 Khanymey and October in Stordalen) because, even if seasons are known to play an import role
383 in the BDOC, it has been shown that BDOC generally decreases as the Arctic summer progress
384 (Holmes et al., 2008; Mann et al., 2012; Vonk et al., 2015; Wickland et al., 2012). Therefore,
385 the effect of seasons would produce an opposite effect to that observed in this study. Moreover,
386 the PCA revealed that the BDOC₁₅ is not correlated to the TBC (Figure 4). Thus, given the
387 higher values of BDOC₁₅ and the lower values of TBC in Stordalen compared with Khanymey,
388 we hypothesize that the biodiversity of microorganisms in the experiment, rather than the
389 microbial number (TBC) impact the final BDOC of waters. It has been shown that the microbial
390 community drastically and rapidly changes between summer and winter period with a
391 syntrophic winter community having a higher potential for mobilizing and converting complex
392 organic matter to more labile C sources (Vigneron et al., 2019). Consistent with this
393 observation, our results show a smaller increase in the SUVA₂₅₄ (reflecting the presence of
394 aromatic components, Hood et al. (2005); Neff et al. (2006)) during incubation of waters from
395 Stordalen (12 to 22% increase) compared to Khanymey (14 to 58% increase) (Figure 2 C). In
396 comparison, the biodegradation of peat water from the European boreal zone using the
397 experimental approach similar to that of the present study, produced an increase in SUVA₂₅₄
398 by 7.4 ± 4.2 % (Hulatt et al., 2014).

399

400 4.4 How does CO₂ production from experimental DOC biodegradation relate to field-
401 based fluxes estimates

402 The findings of this study and widely reported dominance of low-biodegradable DOC
403 (0-15% BDOC) in large rivers and streams of the discontinuous permafrost zone (Frey et al.,
404 2016; Vonk et al., 2015) suggest that 1) the majority of DOC is degraded before its arrival to
405 large aquatic reservoirs (Striegl et al., 2005), and 2) the CO₂ supersaturation and emission of
406 surface waters of frozen peatlands can be largely a result of soil, soil pore water and sediment
407 respiration rather than an aerobic bio- and photo-degradation of DOM in the water column
408 (Audry et al., 2011; Deshpande et al., 2017; Rocher-Ros et al., 2020; Shirokova et al., 2019).

409 In order to quantify the potential importance of biodegradation of DOC to the
410 atmospheric CO₂ fluxes from the study systems, we assumed that the entire consumed DOC
411 was converted into CO₂. This assumption allows to determine the maximal CO₂ emission
412 possible due to the biodegradation, keeping in mind that the true value is likely lower. Thus, to
413 assess the amount of CO₂, potentially emitted due to the total mineralization of OC *via*
414 biodegradation (RCO₂) in each water body, we multiplied RDOC₁₅ (Table S5) by the mean
415 depth of the water columns (Table S1). This calculation assumes 1) negligible uptake of C for
416 bacterial biomass growth, 2) constant biodegradation intensity over the full depth of the water
417 column, and that 3) the entire DOC pool is available for degradation. The obtained RCO₂ values
418 decreased for both HC from headwaters to streams and rivers of both Khanymey (range: -33 ±
419 45 to 241 ± 72 mg C-CO₂ m⁻² d⁻¹) and the Stordalen (9 ± 3 to 359 ± 63 mg C-CO₂ m⁻² d⁻¹) HC
420 (Figure 5). The median (± IQR) RCO₂ values of thaw ponds and lakes of the Khanymey site
421 (169 ± 72 mg C-CO₂ m⁻² d⁻¹, data not shown) are sizably lower than the median CO₂ emissions
422 from the western Siberia lowland (WSL) thermokarst lakes measured by floating chambers
423 (1,101 ± 4,150 mg C-CO₂ m⁻² d⁻¹, Serikova et al. (2019)). The RCO₂ of the Khanymey streams
424 and river (49 ± 68 mg C-CO₂ m⁻² d⁻¹, data not shown) are also much lower than the median

425 values of CO₂ emissions from the WSL rivers ($6,000 \pm 3,900$ mg C-CO₂ m⁻² d⁻¹, [Serikova et al.](#)
426 [\(2018\)](#)). Similarly, the median RCO₂ of pond, fen and lake of the Stordalen site (38 ± 62 mg
427 C-CO₂ m⁻² d⁻¹, data not shown) are much lower than the median CO₂ emissions from small (4-
428 150 m²) thaw ponds of this mire ($3,348 \pm 1,392$ mg C-CO₂ m⁻² d⁻¹, [Kuhn et al. \(2018\)](#)). This
429 comparison clearly demonstrates that the potential contribution of DOC biodegradation to the
430 field-measured CO₂ emissions from inland waters of permafrost peatlands is typically below
431 10 % (Figure 5).

432 Therefore, the DOC biodegradation rates obtained in this study for the water column appear to
433 be insufficient to support the observed CO₂ emissions from the water surface to the atmosphere.
434 Several factors can contribute to this disparity. First, aerobic and anaerobic respiration of
435 stream, lake and river sediments as well as soil water input *via* supra-permafrost flow (i.e.,
436 [Raudina et al., 2018](#)), that can produce a sizeable amount of CO₂, thus increasing overall C
437 emission potential of the aquatic systems ([MacIntyre et al., 2018](#); [Valle et al., 2018](#)). For
438 example, anaerobic C mineralization of thermokarst lake sediments is fairly well established in
439 discontinuous permafrost zone of peat bogs in western Siberia ([Audry et al., 2011](#)) and Canada
440 ([Deshpande et al., 2017](#)). Second, the photo-degradation ([Panneer Selvam et al., 2019](#)) of OM
441 as well as the photo-stimulation of the microbial respiration, which is known to decrease along
442 the HC ([Cory and Kling, 2018](#)), could enhance natural CO₂ emission compared to laboratory
443 incubations. Third, the POC present in the water column in the field can sizably contribute to
444 overall CO₂ emissions from surface waters: it has been shown that, during laboratory
445 incubations of boreal and subarctic waters, the POC is 15 times more reactive towards
446 biodegradation than DOC ([Attermeyer et al., 2018](#)).

447 Our study dealt solely with dissolved components in closed systems and was conducted
448 in the ice-free season of arctic peatlands. Although the results of both incubations are
449 comparable between sites, which were sampled during the baseflow summer-autumn period,

450 additional factors need to be considered in order to fully understand the biogeochemical
451 processing of organic carbon in natural systems. These include i) seasonality (Gao et al., 2019;
452 Kaiser et al., 2017; Li et al., 2019), notably spring snowmelt period (Tang et al., 2018) and
453 potential anoxic conditions in summer and winter (Deshpande et al., 2017), ii) water retention
454 time (Moore, 2009; Olefeldt and Roulet, 2012; Tang et al., 2018), iii) vegetation cover which
455 affects quality and quantity of OM input (Gałka et al., 2017; Kaiser et al., 2017); iv) the ratio
456 of water volume to soil/sediment surface area which determines the rate of fresh OM input
457 (Polishchuk et al., 2017), v) the biodegradability of the particulate organic carbon (Attermeyer
458 et al., 2018), and vi) redox conditions in the water column (Deshpande et al., 2017) and at the
459 water-sediment interface (Valle et al., 2018).

460 **5. Conclusions**

461 Biodegradation experiments demonstrated a decreasing trend of DOC removal rate
462 along the HC from soil solutions to lakes, streams, and rivers of the discontinuous permafrost
463 zone of permafrost peatlands of W. Siberia and N. Sweden. While we hypothesized a decrease
464 of the DOC biodegradability along the HC, the BDOC increased from the beginning to the end
465 of the continuum. This could be linked to preferential removal of labile, low molecular weight
466 compartments of the DOM which are likely to be firstly processed during the transition because
467 the fresher DOC is delivered into the early stages of the HC. Low DOM biodegradability
468 reported in this study (0 and 20%) suggests that the majority of BDOC is degraded before its
469 arrival to a larger aquatic reservoir or even before reaching surface waters. We also suggest that
470 the biodegradation can support part of the CO₂ emissions from surface waters of these peatlands
471 but that other sources are likely of larger importance, including soil and sediment respiration of
472 dissolved and particulate OC, photo-degradation and photo-stimulation of the microbial
473 respiration. Concurrent measurements of BDOC and direct CO₂ emissions in the field are
474 needed to constrain the quantitative importance of *in-situ* DOM degradation for CO₂ fluxes to
475 the atmosphere. Considering the fast processing of OM at the beginning of the continuum and
476 the increasing biodegradability of waters along the HC, this study highlights the importance of
477 accounting for the large spatial heterogeneity of aquatic environments which is needed for
478 mechanistically modeling of C cycling in permafrost peatlands.

479 **CRedit authorship contribution statement**

480 **D. Payandi-Rolland:** conceptualization, investigation, writing – original draft, **L.S.**
481 **Shirokova:** conceptualization, investigation, writing – original draft, **M. Tesfa:** investigation,
482 **P. Bénézech:** writing – original draft, **A.G. Lim:** investigation, **D. Kuzmina:** investigation, **J.**
483 **Karlsson:** conceptualization, writing – original draft, **R. Giesler:** conceptualization, writing –
484 original draft, **O.S. Pokrovsky:** conceptualization, writing – original draft.

485

486 **Acknowledgments**

487 The fieldwork in Siberia was supported by the international program INTERACT for the 2018
488 campaign (“BIOCARSIB”), the Russian Fund for Basic Research grant no. 19-29-05209-mk,
489 and Russian Scientific Fund project No 18-77-10045 (fieldwork in Khanymey). The fieldwork
490 in Sweden was supported by the international project for mobility funded by the University
491 Paul Sabatier (Toulouse 3, France) (“BioCarZA”) and by the Swedish Research Council (grant
492 no. 2016-05275). **D.P-R** was supported by a Ph. D. fellowship from the French « Ministère de
493 l’Enseignement Supérieur, de la Recherche et de l’Innovation ». **M.T** was supported by the
494 « Axe transverse – AST GES » of the Observatoire Midi-Pyrénées. We thank our colleagues
495 from the Tomsk State University (TSU) for the logistic and help during the Siberian field trip.
496 We thank the Climate Impacts Research Centre (CIRC), Umeå University, for hosting the
497 Swedish experimental part of this research. We are grateful to Carole Causserand (GET) for
498 help with DIC and DOC concentrations analyses, Frédéric Julien (EcoLab) for Dionex HPLC
499 measurements of anions and organic acids, and Joey Allen (Ecolab) as well as Joséphine
500 Leflaive (Ecolab) for the help on flow cytometry.

501

502 **Conflicts of interests**

503 The authors declare no conflict of interest.

References

- 506 Abbott, B.W., Jones, J.B., Schuur, E.A.G., III, F.S.C., Bowden, W.B., Bret-Harte, M.S.,
 507 Epstein, H.E., Flannigan, M.D., Harms, T.K., Hollingsworth, T.N., Mack, M.C.,
 508 McGuire, A.D., Natali, S.M., Rocha, A.V., Tank, S.E., Turetsky, M.R., Vonk, J.E.,
 509 Wickland, K.P., Aiken, G.R., Alexander, H.D., Amon, R.M.W., Benscoter, B.W.,
 510 Bergeron, Y., Bishop, K., Blarquez, O., Bond-Lamberty, B., Breen, A.L., Buffam, I.,
 511 Cai, Y., Carcaillet, C., Carey, S.K., Chen, J.M., Chen, H.Y.H., Christensen, T.R.,
 512 Cooper, L.W., Cornelissen, J.H.C., Groot, W.J. de, DeLuca, T.H., Dorrepaal, E.,
 513 Fetcher, N., Finlay, J.C., Forbes, B.C., French, N.H.F., Gauthier, S., Girardin, M.P.,
 514 Goetz, S.J., Goldammer, J.G., Gough, L., Grogan, P., Guo, L., Higuera, P.E.,
 515 Hinzman, L., Hu, F.S., Hugelius, G., Jafarov, E.E., Jandt, R., Johnstone, J.F.,
 516 Karlsson, J., Kasischke, E.S., Kattner, G., Kelly, R., Keuper, F., Kling, G.W.,
 517 Kortelainen, P., Kouki, J., Kuhry, P., Laudon, H., Laurion, I., Macdonald, R.W.,
 518 Mann, P.J., Martikainen, P.J., McClelland, J.W., Molau, U., Oberbauer, S.F., Olefeldt,
 519 D., Paré, D., Parisien, M.-A., Payette, S., Peng, C., Pokrovsky, O.S., Rastetter, E.B.,
 520 Raymond, P.A., Reynolds, M.K., Rein, G., Reynolds, J.F., Robards, M., Rogers, B.M.,
 521 Schädel, C., Schaefer, K., Schmidt, I.K., Shvidenko, A., Sky, J., Spencer, R.G.M.,
 522 Starr, G., Striegl, R.G., Teisserenc, R., Tranvik, L.J., Virtanen, T., Welker, J.M.,
 523 Zimov, S., 2016. Biomass offsets little or none of permafrost carbon release from
 524 soils, streams, and wildfire: an expert assessment. *Environ. Res. Lett.* 11, 034014.
 525 <https://doi.org/10.1088/1748-9326/11/3/034014>
- 526 Abbott, B.W., Larouche, J.R., Jones, J.B., Bowden, W.B., Balser, A.W., 2014. Elevated
 527 dissolved organic carbon biodegradability from thawing and collapsing permafrost:
 528 Permafrost carbon biodegradability. *J. Geophys. Res. Biogeosciences* 119, 2049–
 529 2063. <https://doi.org/10.1002/2014JG002678>
- 530 Åkerman, H.J., Johansson, M., 2008. Thawing permafrost and thicker active layers in sub-
 531 arctic Sweden. *Permafr. Periglac. Process.* 19, 279–292.
 532 <https://doi.org/10.1002/ppp.626>
- 533 Ala-aho, P., Soulsby, C., Pokrovsky, O.S., Kirpotin, S.N., Karlsson, J., Serikova, S.,
 534 Manasypov, R., Lim, A., Krickov, I., Kolesnichenko, L.G., Laudon, H., Tetzlaff, D.,
 535 2018. Permafrost and lakes control river isotope composition across a boreal Arctic
 536 transect in the Western Siberian lowlands. *Environ. Res. Lett.* 13, 034028.
 537 <https://doi.org/10.1088/1748-9326/aaa4fe>
- 538 Attermeyer, K., Catalán, N., Einarsdottir, K., Freixa, A., Groeneveld, M., Hawkes, J.A.,
 539 Bergquist, J., Tranvik, L.J., 2018. Organic Carbon Processing During Transport
 540 Through Boreal Inland Waters: Particles as Important Sites. *J. Geophys. Res.*
 541 *Biogeosciences*. <https://doi.org/10.1029/2018JG004500>
- 542 Audry, S., Pokrovsky, O.S., Shirokova, L.S., Kirpotin, S.N., Dupré, B., 2011. Organic matter
 543 mineralization and trace element post-depositional redistribution in Western Siberia
 544 thermokarst lake sediments. *Biogeosciences* 8, 3341–3358. <https://doi.org/10.5194/bg-8-3341-2011>
- 546 Brown, J., Ferrians Jr, O., Heginbottom, J., Melnikov, E., 1997. Circum-Arctic map of
 547 permafrost and ground-ice conditions. US Geological Survey Reston, VA.
- 548 Cappenberg, T.E., Hordijk, K.A., Jonkheer, G.J., Lauwen, J.P.M., 1982. Carbon flow across
 549 the sediment-water interface in Lake Vechten, The Netherlands. *Hydrobiologia* 91,
 550 161–168. <https://doi.org/10.1007/BF02391932>

551 Catalán, N., Marcé, R., Kothawala, D.N., Tranvik, L.J., 2016. Organic carbon decomposition
552 rates controlled by water retention time across inland waters. *Nat. Geosci.* 9, 501–504.
553 <https://doi.org/10.1038/ngeo2720>

554 Chapin, F.S., Woodwell, G.M., Randerson, J.T., Rastetter, E.B., Lovett, G.M., Baldocchi,
555 D.D., Clark, D.A., Harmon, M.E., Schimel, D.S., Valentini, R., Wirth, C., Aber, J.D.,
556 Cole, J.J., Goulden, M.L., Harden, J.W., Heimann, M., Howarth, R.W., Matson, P.A.,
557 McGuire, A.D., Melillo, J.M., Mooney, H.A., Neff, J.C., Houghton, R.A., Pace, M.L.,
558 Ryan, M.G., Running, S.W., Sala, O.E., Schlesinger, W.H., Schulze, E.-D., 2006.
559 Reconciling Carbon-cycle Concepts, Terminology, and Methods. *Ecosystems* 9,
560 1041–1050. <https://doi.org/10.1007/s10021-005-0105-7>

561 Chupakov, A.V., Pokrovsky, O.S., Moreva, O.Y., Shirokova, L.S., Neverova, N.V.,
562 Chupakova, A.A., Kotova, E.I., Vorobyeva, T.Y., 2020. High resolution multi-annual
563 riverine fluxes of organic carbon, nutrient and trace element from the largest European
564 Arctic river, Severnaya Dvina. *Chem. Geol.* 538, 119491.
565 <https://doi.org/10.1016/j.chemgeo.2020.119491>

566 Cole, J.J., Prairie, Y.T., Caraco, N.F., McDowell, W.H., Tranvik, L.J., Striegl, R.G., Duarte,
567 C.M., Kortelainen, P., Downing, J.A., Middelburg, J.J., Melack, J., 2007. Plumbing
568 the Global Carbon Cycle: Integrating Inland Waters into the Terrestrial Carbon
569 Budget. *Ecosystems* 10, 172–185. <https://doi.org/10.1007/s10021-006-9013-8>

570 Cory, R.M., Kling, G.W., 2018. Interactions between sunlight and microorganisms influence
571 dissolved organic matter degradation along the aquatic continuum. *Limnol. Oceanogr.*
572 *Lett.* 3, 102–116. <https://doi.org/10.1002/lol2.10060>

573 Cory, R.M., Miller, M.P., McKnight, D.M., Guerard, J.J., Miller, P.L., 2010. Effect of
574 instrument-specific response on the analysis of fulvic acid fluorescence spectra.
575 *Limnol. Oceanogr. Methods* 8, 67–78. <https://doi.org/10.4319/lom.2010.8.67>

576 Creed, I.F., McKnight, D.M., Pellerin, B.A., Green, M.B., Bergamaschi, B.A., Aiken, G.R.,
577 Burns, D.A., Findlay, S.E.G., Shanley, J.B., Striegl, R.G., Aulenbach, B.T., Clow,
578 D.W., Laudon, H., McGlynn, B.L., McGuire, K.J., Smith, R.A., Stackpoole, S.M.,
579 2015. The river as a chemostat: fresh perspectives on dissolved organic matter flowing
580 down the river continuum. *Can. J. Fish. Aquat. Sci.* 72, 1272–1285.
581 <https://doi.org/10.1139/cjfas-2014-0400>

582 Demars, B.O.L., 2019. Hydrological pulses and burning of dissolved organic carbon by
583 stream respiration. *Limnol. Oceanogr.* 64, 406–421. <https://doi.org/10.1002/lno.11048>

584 Deshpande, B.N., Maps, F., Matveev, A., Vincent, W.F., 2017. Oxygen depletion in subarctic
585 peatland thaw lakes. *Arct. Sci.* 3, 406–428. <https://doi.org/10.1139/as-2016-0048>

586 Evans, C.D., Futter, M.N., Moldan, F., Valinia, S., Frogbrook, Z., Kothawala, D.N., 2017.
587 Variability in organic carbon reactivity across lake residence time and trophic
588 gradients. *Nat. Geosci.* 10, 832–835. <https://doi.org/10.1038/ngeo3051>

589 Frey, K.E., Sobczak, W.V., Mann, P.J., Holmes, R.M., 2016. Optical properties and
590 bioavailability of dissolved organic matter along a flow-path continuum from soil pore
591 waters to the Kolyma River mainstem, East Siberia. *Biogeosciences* 13, 2279–2290.
592 <https://doi.org/10.5194/bg-13-2279-2016>

593 Gao, T., Kang, S., Chen, R., Zhang, Taigang, Zhang, Tingjun, Han, C., Tripathi, L.,
594 Sillanpää, M., Zhang, Y., 2019. Riverine dissolved organic carbon and its optical
595 properties in a permafrost region of the Upper Heihe River basin in the Northern
596 Tibetan Plateau. *Sci. Total Environ.* 686, 370–381.
597 <https://doi.org/10.1016/j.scitotenv.2019.05.478>

598 Holmes, R.M., McClelland, J.W., Peterson, B.J., Tank, S.E., Bulygina, E., Eglinton, T.I.,
599 Gordeev, V.V., Gurtovaya, T.Y., Raymond, P.A., Repeta, D.J., Staples, R., Striegl,
600 R.G., Zhulidov, A.V., Zimov, S.A., 2012. Seasonal and Annual Fluxes of Nutrients

601 and Organic Matter from Large Rivers to the Arctic Ocean and Surrounding Seas.
602 *Estuaries Coasts* 35, 369–382. <https://doi.org/10.1007/s12237-011-9386-6>

603 Holmes, R.M., McClelland, J.W., Raymond, P.A., Frazer, B.B., Peterson, B.J., Stieglitz, M.,
604 2008. Lability of DOC transported by Alaskan rivers to the Arctic Ocean. *Geophys.*
605 *Res. Lett.* 35. <https://doi.org/10.1029/2007GL032837>

606 Hood, E., Williams, M.W., McKnight, D.M., 2005. Sources of dissolved organic matter
607 (DOM) in a Rocky Mountain stream using chemical fractionation and stable isotopes.
608 *Biogeochemistry* 74, 231–255. <https://doi.org/10.1007/s10533-004-4322-5>

609 Hulatt, C.J., Kaartokallio, H., Asmala, E., Autio, R., Stedmon, C.A., Sonninen, E., Oinonen,
610 M., Thomas, D.N., 2014. Bioavailability and radiocarbon age of fluvial dissolved
611 organic matter (DOM) from a northern peatland-dominated catchment: effect of land-
612 use change. *Aquat. Sci.* 76, 393–404. <https://doi.org/10.1007/s00027-014-0342-y>

613 Hutchins, R.H.S., Aukes, P., Schiff, S.L., Dittmar, T., Prairie, Y.T., Giorgio, P.A. del, 2017.
614 The Optical, Chemical, and Molecular Dissolved Organic Matter Succession Along a
615 Boreal Soil-Stream-River Continuum. *J. Geophys. Res. Biogeosciences* 122, 2892–
616 2908. <https://doi.org/10.1002/2017JG004094>

617 Kawasaki, N., Komatsu, K., Kohzu, A., Tomioka, N., Shinohara, R., Satou, T., Watanabe,
618 F.N., Tada, Y., Hamasaki, K., Kushairi, M.R.M., Imai, A., 2013. Bacterial
619 Contribution to Dissolved Organic Matter in Eutrophic Lake Kasumigaura, Japan.
620 *Appl. Environ. Microbiol.* 79, 7160–7168. <https://doi.org/10.1128/AEM.01504-13>

621 Kirpotin, S.N., Berezin, A., Bazanov, V., Polishchuk, Y., Vorobiov, S., Mironycheva-
622 Tokoreva, N., Kosykh, N., Volkova, I., Dupre, B., Pokrovsky, O., Kouraev, A.,
623 Zakharova, E., Shirokova, L., Mognard, N., Biancamaria, S., Viers, J., Kolmakova,
624 M., 2009. Western Siberia wetlands as indicator and regulator of climate change on
625 the global scale. *Int. J. Environ. Stud.* 66, 409–421.
626 <https://doi.org/10.1080/00207230902753056>

627 Klaminder, J., Yoo, K., Rydberg, J., Giesler, R., 2008. An explorative study of mercury
628 export from a thawing palsamire. *J. Geophys. Res. Biogeosciences* 113.
629 <https://doi.org/10.1029/2008JG000776>

630 Kohler, J., Brandt, O., Johansson, M., Callaghan, T., 2006. A long-term Arctic snow depth
631 record from Abisko, northern Sweden, 1913–2004. *Polar Res.* 25, 91–113.
632 <https://doi.org/10.3402/polar.v25i2.6240>

633 Kuhn, M., Lundin, E.J., Giesler, R., Johansson, M., Karlsson, J., 2018. Emissions from thaw
634 ponds largely offset the carbon sink of northern permafrost wetlands. *Sci. Rep.* 8,
635 9535. <https://doi.org/10.1038/s41598-018-27770-x>

636 Li, Y., Song, G., Massicotte, P., Yang, F., Li, R., Xie, H., 2019. Distribution, seasonality, and
637 fluxes of dissolved organic matter in the Pearl River (Zhujiang) estuary, China.
638 *Biogeosciences* 16, 2751–2770. <https://doi.org/10.5194/bg-16-2751-2019>

639 Lindström, M., Bax, G., Dinger, M., Dworatzek, M., Erdtmann, W., Fricke, A., Kathol, B.,
640 1985. Geology of a part of the Torneträsk section of the Caledonian front, northern
641 Sweden.

642 Liu, F., Kou, D., Abbott, B.W., Mao, C., Chen, Y., Chen, L., Yang, Y., 2019. Disentangling
643 the Effects of Climate, Vegetation, Soil and Related Substrate Properties on the
644 Biodegradability of Permafrost-Derived Dissolved Organic Carbon. *J. Geophys. Res.*
645 *Biogeosciences* 124, 3377–3389. <https://doi.org/10.1029/2018JG004944>

646 Ma, Q., Jin, H., Yu, C., Bense, V.F., 2019. Dissolved organic carbon in permafrost regions: A
647 review. *Sci. China Earth Sci.* 62, 349–364. <https://doi.org/10.1007/s11430-018-9309-6>

648 MacIntyre, S., Cortés, A., Sadro, S., 2018. Sediment respiration drives circulation and
649 production of CO₂ in ice-covered Alaskan arctic lakes. *Limnol. Oceanogr. Lett.* 3,
650 302–310. <https://doi.org/10.1002/lo12.10083>

651 Malmer, N., Johansson, T., Olsrud, M., Christensen, T.R., 2005. Vegetation, climatic changes
652 and net carbon sequestration in a North-Scandinavian subarctic mire over 30 years.
653 *Glob. Change Biol.* 11, 1895–1909. <https://doi.org/10.1111/j.1365-2486.2005.01042.x>
654 Manasypov, R.M., Vorobyev, S.N., Loiko, S.V., Kritzkov, I.V., Shirokova, L.S., Shevchenko,
655 V.P., Kirpotin, S.N., Kulizhsky, S.P., Kolesnichenko, L.G., Zemtzov, V.A., Sinkinov,
656 V.V., Pokrovsky, O.S., 2015. Seasonal dynamics of organic carbon and metals in
657 thermokarst lakes from the discontinuous permafrost zone of western Siberia.
658 *Biogeosciences* 12, 3009–3028. <https://doi.org/10.5194/bg-12-3009-2015>
659 Mann, P.J., Davydova, A., Zimov, N., Spencer, R.G.M., Davydov, S., Bulygina, E., Zimov,
660 S., Holmes, R.M., 2012. Controls on the composition and lability of dissolved organic
661 matter in Siberia’s Kolyma River basin. *J. Geophys. Res. Biogeosciences* 117.
662 <https://doi.org/10.1029/2011JG001798>
663 Mann, P.J., Eglinton, T.I., McIntyre, C.P., Zimov, N., Davydova, A., Vonk, J.E., Holmes,
664 R.M., Spencer, R.G.M., 2015. Utilization of ancient permafrost carbon in headwaters
665 of Arctic fluvial networks. *Nat. Commun.* 6, 7856.
666 <https://doi.org/10.1038/ncomms8856>
667 McKnight, D.M., Boyer, E.W., Westerhoff, P.K., Doran, P.T., Kulbe, T., Andersen, D.T.,
668 2001. Spectrofluorometric characterization of dissolved organic matter for indication
669 of precursor organic material and aromaticity. *Limnol. Oceanogr.* 46, 38–48.
670 <https://doi.org/10.4319/lo.2001.46.1.0038>
671 Michaelson, G.J., Ping, C.L., Kling, G.W., Hobbie, J.E., 1998. The character and bioactivity
672 of dissolved organic matter at thaw and in the spring runoff waters of the arctic tundra
673 North Slope, Alaska. *J. Geophys. Res. Atmospheres* 103, 28939–28946.
674 <https://doi.org/10.1029/98JD02650>
675 Neff, J.C., Finlay, J.C., Zimov, S.A., Davydov, S.P., Carrasco, J.J., Schuur, E. a. G.,
676 Davydova, A.I., 2006. Seasonal changes in the age and structure of dissolved organic
677 carbon in Siberian rivers and streams. *Geophys. Res. Lett.* 33.
678 <https://doi.org/10.1029/2006GL028222>
679 Obernosterer, I., Benner, R., 2004. Competition between biological and photochemical
680 processes in the mineralization of dissolved organic carbon. *Limnol. Oceanogr.* 49,
681 117–124. <https://doi.org/10.4319/lo.2004.49.1.0117>
682 Olefeldt, D., Roulet, N.T., 2014. Permafrost conditions in peatlands regulate magnitude,
683 timing, and chemical composition of catchment dissolved organic carbon export.
684 *Glob. Change Biol.* 20, 3122–3136. <https://doi.org/10.1111/gcb.12607>
685 Olefeldt, D., Roulet, N.T., 2012. Effects of permafrost and hydrology on the composition and
686 transport of dissolved organic carbon in a subarctic peatland complex. *J. Geophys.*
687 *Res. Biogeosciences* 117. <https://doi.org/10.1029/2011JG001819>
688 Palmer, S.M., Evans, C.D., Chapman, P.J., Burden, A., Jones, T.G., Allott, T.E.H., Evans,
689 M.G., Moody, C.S., Worrall, F., Holden, J., 2016. Sporadic hotspots for physico-
690 chemical retention of aquatic organic carbon: from peatland headwater source to sea.
691 *Aquat. Sci.* 78, 491–504. <https://doi.org/10.1007/s00027-015-0448-x>
692 Panneer Selvam, B., Lapiere, J.-F., Soares, A.R.A., Bastviken, D., Karlsson, J., Berggren,
693 M., 2019. Photo-reactivity of dissolved organic carbon in the freshwater continuum.
694 *Aquat. Sci.* 81, 57. <https://doi.org/10.1007/s00027-019-0653-0>
695 Payandi-Rolland, D., 2020. Data from the DOM biodegradation along a hydrological
696 continuum in permafrost peatlands. <https://doi.org/10.17632/K9J72KJ6JS.1>
697 Peacock, M., Evans, C.D., Fenner, N., Freeman, C., Gough, R., Jones, T.G., Lebron, I., 2014.
698 UV-visible absorbance spectroscopy as a proxy for peatland dissolved organic carbon
699 (DOC) quantity and quality: considerations on wavelength and absorbance

700 degradation. *Environ. Sci. Process. Impacts* 16, 1445–1461.
701 <https://doi.org/10.1039/C4EM00108G>

702 Petrescu, A.M.R., Van Huissteden, J.C., Jackowicz-Korczynski, M., Yurova, A., Christensen,
703 T.R., Crill, P.M., Maximov, T.C., 2007. Modelling CH₄ emissions from arctic
704 wetlands: effects of hydrological parameterization. *Biogeosciences Discuss.* 4, 3195–
705 3227.

706 Peura, S., Wauthy, M., Simone, D., Eiler, A., Einarsdóttir, K., Rautio, M., Bertilsson, S.,
707 2020. Ontogenic succession of thermokarst thaw ponds is linked to dissolved organic
708 matter quality and microbial degradation potential. *Limnol. Oceanogr.* 65, S248–S263.
709 <https://doi.org/10.1002/lno.11349>

710 Pokrovsky, O.S., Manasypov, R.M., Loiko, S.V., Shirokova, L.S., 2016. Organic and organo-
711 mineral colloids in discontinuous permafrost zone. *Geochim. Cosmochim. Acta* 188,
712 1–20. <https://doi.org/10.1016/j.gca.2016.05.035>

713 Pokrovsky, O.S., Shirokova, L.S., Kirpotin, S.N., Audry, S., Viers, J., Dupré, B., 2011. Effect
714 of permafrost thawing on organic carbon and trace element colloidal speciation in the
715 thermokarst lakes of western Siberia. *Biogeosciences* 8, 565–583.
716 <https://doi.org/10.5194/bg-8-565-2011>

717 Raudina, T.V., Loiko, S.V., Lim, A., Manasypov, R.M., Shirokova, L.S., Istigechev, G.I.,
718 Kuzmina, D.M., Kulizhsky, S.P., Vorobyev, S.N., Pokrovsky, O.S., 2018. Permafrost
719 thaw and climate warming may decrease the CO₂, carbon, and metal concentration in
720 peat soil waters of the Western Siberia Lowland. *Sci. Total Environ.* 634, 1004–1023.
721 <https://doi.org/10.1016/j.scitotenv.2018.04.059>

722 Rocher-Ros, G., Sponseller, R.A., Bergström, A.-K., Myrstener, M., Giesler, R., 2020. Stream
723 metabolism controls diel patterns and evasion of CO₂ in Arctic streams. *Glob. Change*
724 *Biol.* 26, 1400–1413. <https://doi.org/10.1111/gcb.14895>

725 Roehm, C.L., Giesler, R., Karlsson, J., 2009. Bioavailability of terrestrial organic carbon to
726 lake bacteria: The case of a degrading subarctic permafrost mire complex. *J. Geophys.*
727 *Res. Biogeosciences* 114. <https://doi.org/10.1029/2008JG000863>

728 Serikova, S., Pokrovsky, O.S., Ala-Aho, P., Kazantsev, V., Kirpotin, S.N., Kopysov, S.G.,
729 Krickov, I.V., Laudon, H., Manasypov, R.M., Shirokova, L.S., Soulsby, C., Tetzlaff,
730 D., Karlsson, J., 2018. High riverine CO₂ emissions at the permafrost boundary of
731 Western Siberia. *Nat. Geosci.* 1. <https://doi.org/10.1038/s41561-018-0218-1>

732 Serikova, S., Pokrovsky, O.S., Laudon, H., Krickov, I.V., Lim, A.G., Manasypov, R.M.,
733 Karlsson, J., 2019. High carbon emissions from thermokarst lakes of Western Siberia.
734 *Nat. Commun.* 10, 1552. <https://doi.org/10.1038/s41467-019-09592-1>

735 Shirokova, L.S., Chupakov, A.V., Zabelina, S.A., Neverova, N.V., Payandi-Rolland, D.,
736 Causserand, C., Karlsson, J., Pokrovsky, O.S., 2019. Humic surface waters of frozen
737 peat bogs (permafrost zone) are highly resistant to bio- and photodegradation.
738 *Biogeosciences* 16, 2511–2526. <https://doi.org/10.5194/bg-16-2511-2019>

739 Spencer, R.G.M., Mann, P.J., Dittmar, T., Eglinton, T.I., McIntyre, C., Holmes, R.M., Zimov,
740 N., Stubbins, A., 2015. Detecting the signature of permafrost thaw in Arctic rivers.
741 *Geophys. Res. Lett.* 42, 2830–2835. <https://doi.org/10.1002/2015GL063498>

742 Striegl, R.G., Aiken, G.R., Dornblaser, M.M., Raymond, P.A., Wickland, K.P., 2005. A
743 decrease in discharge-normalized DOC export by the Yukon River during summer
744 through autumn. *Geophys. Res. Lett.* 32. <https://doi.org/10.1029/2005GL024413>

745 Tang, J., Yurova, A.Y., Schurgers, G., Miller, P.A., Olin, S., Smith, B., Siewert, M.B.,
746 Olefeldt, D., Pilesjö, P., Poska, A., 2018. Drivers of dissolved organic carbon export
747 in a subarctic catchment: Importance of microbial decomposition, sorption-desorption,
748 peatland and lateral flow. *Sci. Total Environ.* 622–623, 260–274.
749 <https://doi.org/10.1016/j.scitotenv.2017.11.252>

750 Valle, J., Gonsior, M., Harir, M., Enrich-Prast, A., Schmitt-Kopplin, P., Bastviken, D.,
751 Conrad, R., Hertkorn, N., 2018. Extensive processing of sediment pore water
752 dissolved organic matter during anoxic incubation as observed by high-field mass
753 spectrometry (FTICR-MS). *Water Res.* 129, 252–263.
754 <https://doi.org/10.1016/j.watres.2017.11.015>

755 Vigneron, A., Lovejoy, C., Cruaud, P., Kalenitchenko, D., Culley, A., Vincent, W.F., 2019.
756 Contrasting Winter Versus Summer Microbial Communities and Metabolic Functions
757 in a Permafrost Thaw Lake. *Front. Microbiol.* 10.
758 <https://doi.org/10.3389/fmicb.2019.01656>

759 Vonk, J., Tank, S., Mann, P., Spencer, R., Treat, C., Striegl, R., Abbott, B., Wickland, K.,
760 2015. Biodegradability of dissolved organic carbon in permafrost soils and aquatic
761 systems: a meta-analysis. *Biogeosciences* BG 12, 6915–6930.

762 Vonk, J.E., Gustafsson, Ö., 2013. Permafrost-carbon complexities. *Nat. Geosci.* 6, 675–676.
763 <https://doi.org/10.1038/ngeo1937>

764 Vonk, J.E., Tank, S.E., Walvoord, M.A., 2019. Integrating hydrology and biogeochemistry
765 across frozen landscapes. *Nat. Commun.* 10, 1–4. [https://doi.org/10.1038/s41467-019-](https://doi.org/10.1038/s41467-019-13361-5)
766 13361-5

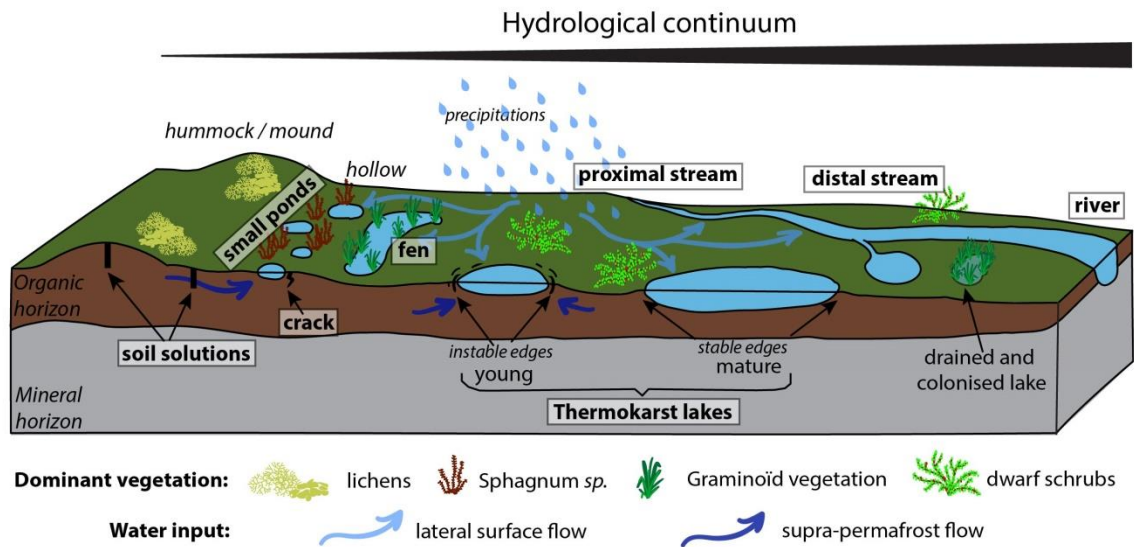
767 Walvoord, M.A., Striegl, R.G., 2007. Increased groundwater to stream discharge from
768 permafrost thawing in the Yukon River basin: Potential impacts on lateral export of
769 carbon and nitrogen. *Geophys. Res. Lett.* 34. <https://doi.org/10.1029/2007GL030216>

770 Weishaar, J.L., Aiken, G.R., Bergamaschi, B.A., Fram, M.S., Fujii, R., Mopper, K., 2003.
771 Evaluation of Specific Ultraviolet Absorbance as an Indicator of the Chemical
772 Composition and Reactivity of Dissolved Organic Carbon. *Environ. Sci. Technol.* 37,
773 4702–4708. <https://doi.org/10.1021/es030360x>

774 Wickland, K.P., Aiken, G.R., Butler, K., Dornblaser, M.M., Spencer, R.G.M., Striegl, R.G.,
775 2012. Biodegradability of dissolved organic carbon in the Yukon River and its
776 tributaries: Seasonality and importance of inorganic nitrogen: BIODEGRADABLE
777 DOC IN THE YUKON RIVER. *Glob. Biogeochem. Cycles* 26, n/a-n/a.
778 <https://doi.org/10.1029/2012GB004342>

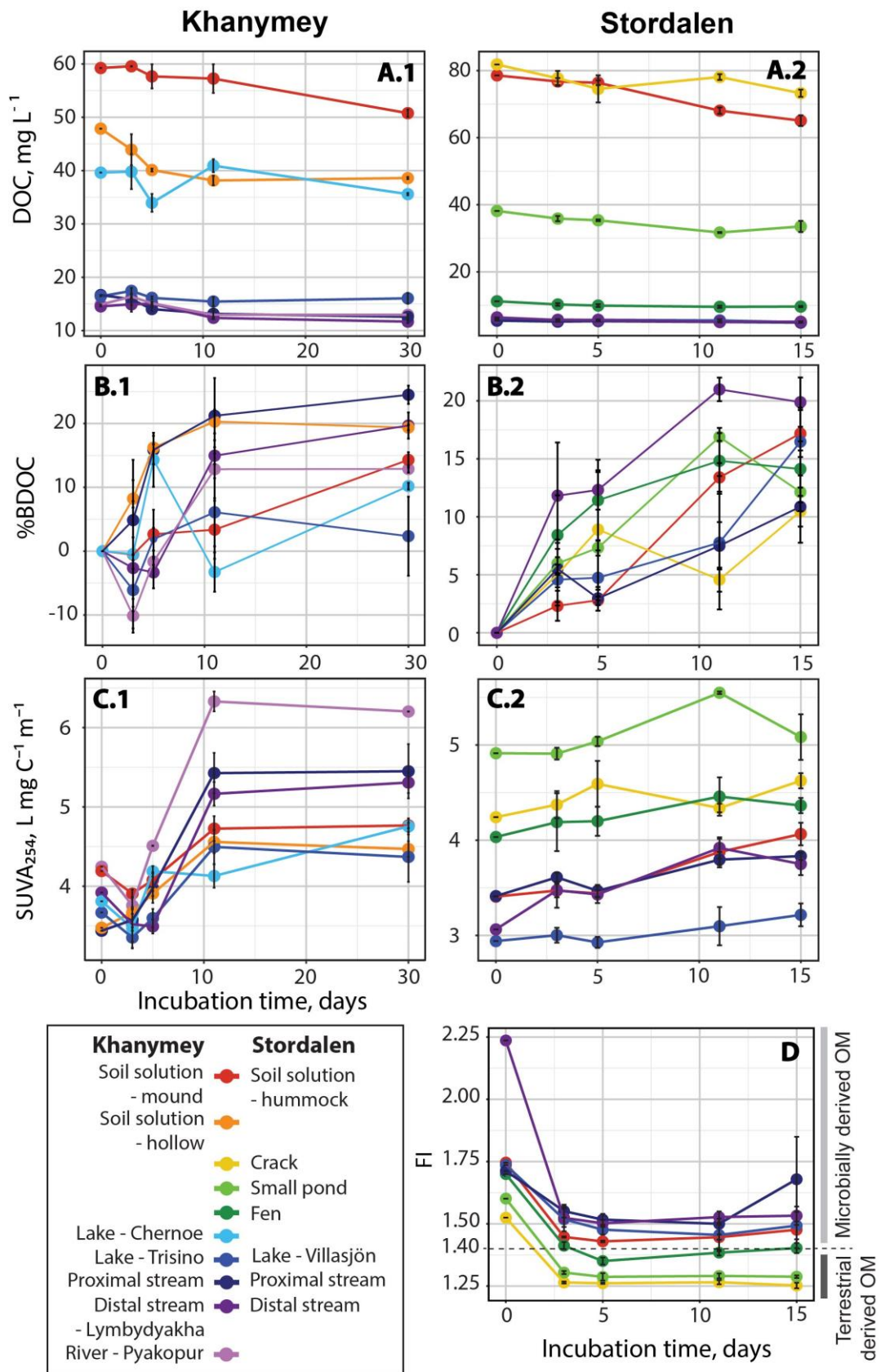
779 Wickland, K.P., Neff, J.C., Aiken, G.R., 2007. Dissolved Organic Carbon in Alaskan Boreal
780 Forest: Sources, Chemical Characteristics, and Biodegradability. *Ecosystems* 10,
781 1323–1340. <https://doi.org/10.1007/s10021-007-9101-4>

782 Wik, M., Crill, P.M., Varner, R.K., Bastviken, D., 2013. Multiyear measurements of ebullitive
783 methane flux from three subarctic lakes. *J. Geophys. Res. Biogeosciences* 118, 1307–
784 1321. <https://doi.org/10.1002/jgrg.20103>
785
786



788

789 **Figure 1:** Schematic of a hydrological continuum in the discontinuous permafrost region. The
 790 hydrological continuum represents a progression of wetland water habitats from gravitational
 791 soil water in soil pits and cracks to small ponds, fens, lakes, streams and rivers. While the soil
 792 solutions represent the upper end of the continuum the rivers are the receiving system at the
 793 other end of the transition. Note that either the vertical or horizontal scales are not
 794 representative.



795

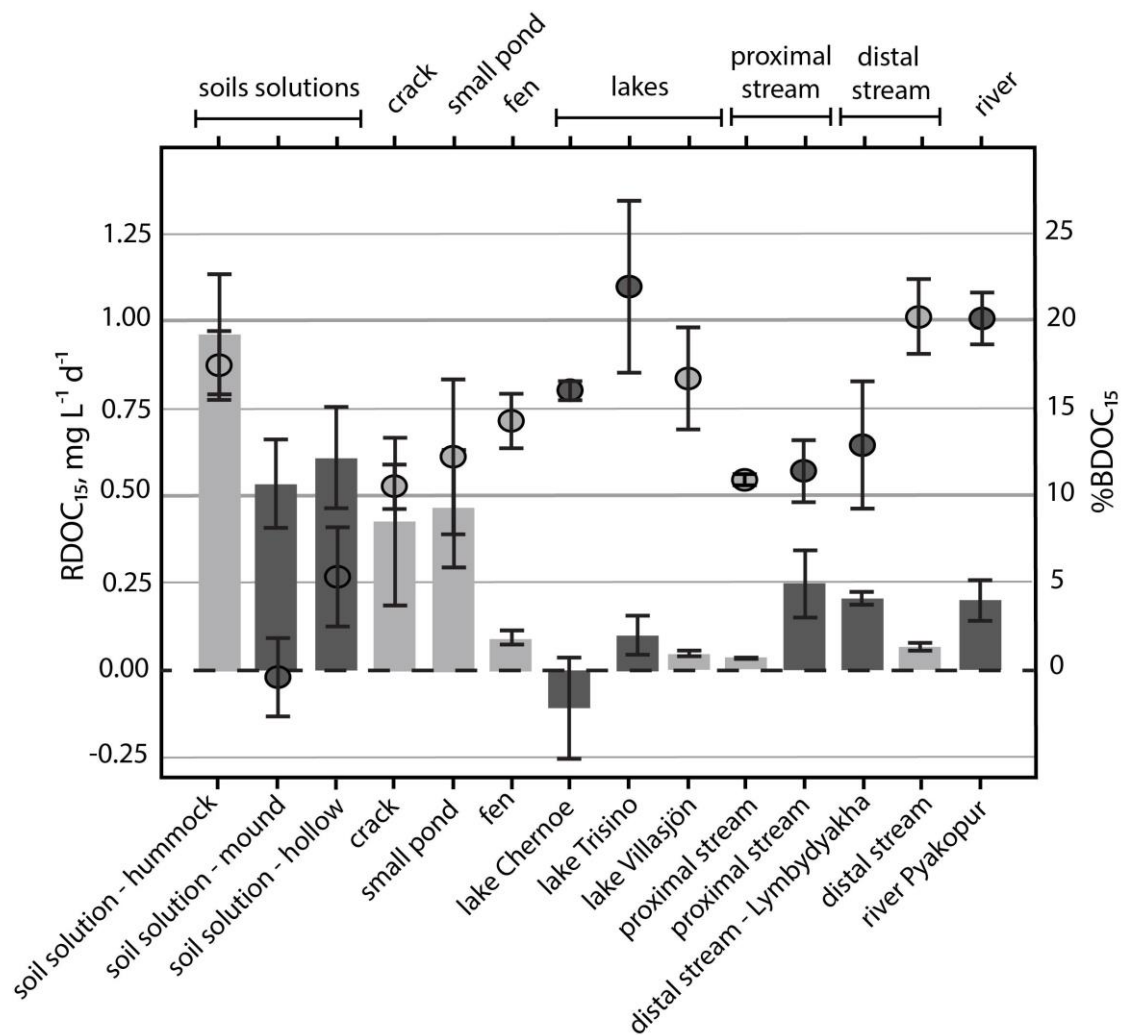
796

797

798

799

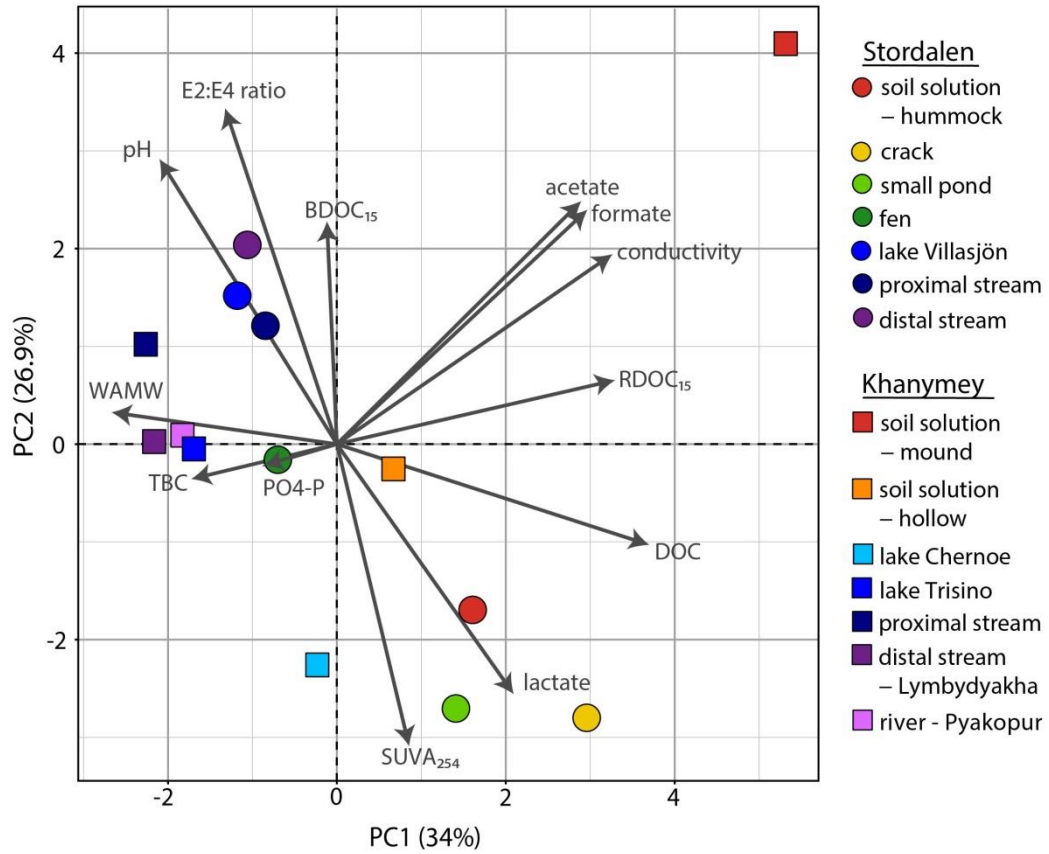
Figure 2: DOC concentration (mg L⁻¹, **A**), BDOC (% **B**), SUVA (L mg C⁻¹ m⁻¹, **C**) of the Khanymey (.1) and Stordalen (.2) hydrological continuum; and FI evolution of the Stordalen continuum during incubation time (**D**). Note that the total incubation time is 30 days for Khanymey continuum and 15 days for Stordalen continuum.



801

802 **Figure 3:** The removal rate of dissolved organic carbon (RDOC₁₅) of waters along the
 803 hydrological continuum (HC) after 15 days of incubations (bars and left y-axes). The filled
 804 circles show the biodegradable DOC (BDOC₁₅) after 15 days of incubations from the same
 805 HC. The waters are from 15 locations across two HC's: one in northern Sweden (Stordalen;
 806 light grey fill for circle and bars) and one in western Siberia (Khanymey; dark grey for circle
 807 fill and bars). The sites are represented starting from the left with the upper end of the HC and
 808 the receiving systems to the right (see figure 1). The error bars denote one standard deviation.

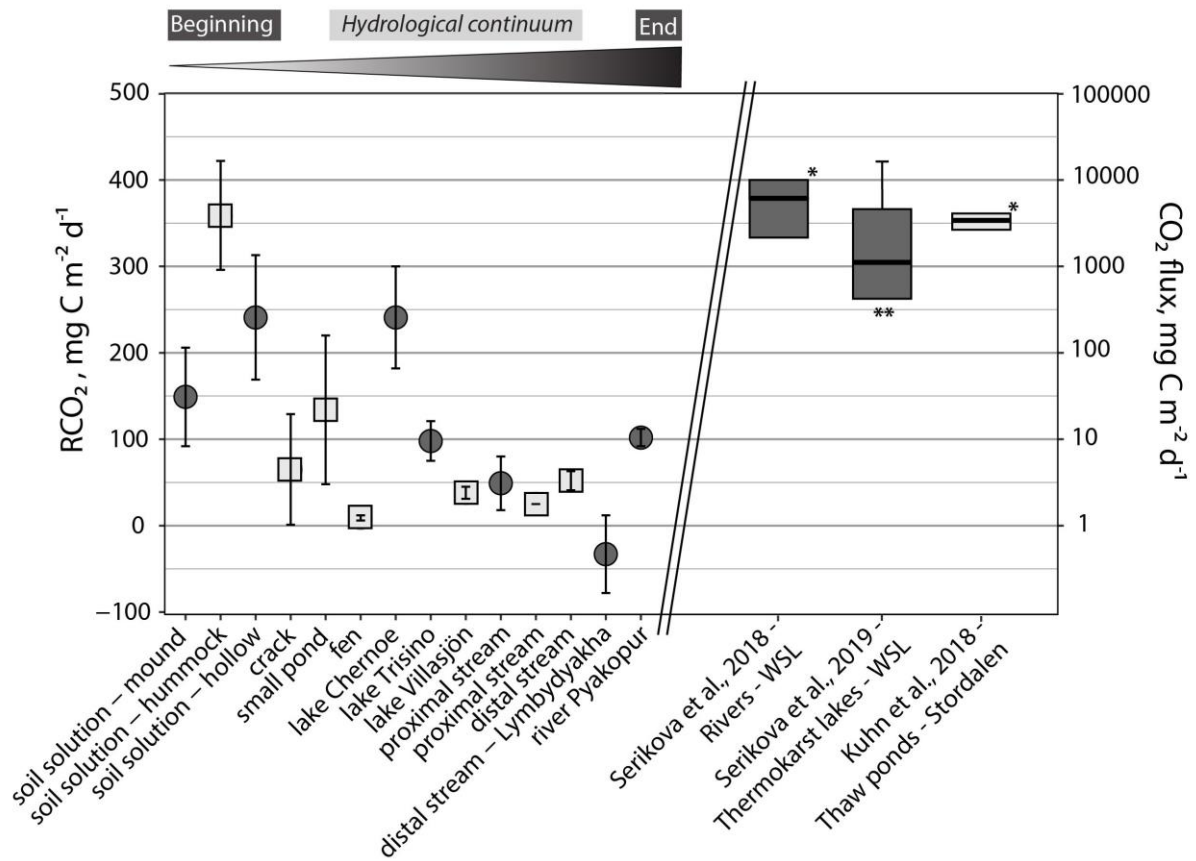
809



810

811 **Figure 4:** Biplot of the individual PCA on waters from Stordalen (circle) and Khanymey
 812 (square) hydrological continuum and variable correlation plot (black arrow).

813



814

815 **Figure 5:** Left axis: Calculated potential CO₂ fluxes (mean ± SD) emitted by biodegradation
 816 (RCO₂) of waters from the Khanymey (black circles) and Stordalen (grey squares)
 817 hydrological continuum. Right axis: CO₂ emissions (mg C m⁻² d⁻¹, log scale) field-based
 818 estimated from other studies in Khanymey region (dark grey boxplot) for rivers (Serikova et
 819 al., 2018) and thermokarst lakes (Serikova et al., 2019) ; and in thaw ponds from the
 820 Stordalen region (light grey boxplot, Kuhn et al. (2018)). The box encloses 50% of the data
 821 and the horizontal bar marks the median. Whiskers extend to the outermost data-points. * No
 822 outermost data-points are given for those studies. ** Negative values for the minimum
 823 outermost data-point